

# Demonstration of a linear optical true-time delay device by use of a microelectromechanical mirror array

Amber Rader and Betty Lise Anderson

We present the design and proof-of-concept demonstration of an optical device capable of producing true-time delay(s) (TTD)(s) for phased array antennas. This TTD device uses a free-space approach consisting of a single microelectromechanical systems (MEMS) mirror array in a multiple reflection spherical mirror configuration based on the White cell. Divergence is avoided by periodic refocusing by the mirrors. By using the MEMS mirror to switch between paths of different lengths, time delays are generated. Six different delays in 1-ns increments were demonstrated by using the Texas Instruments Digital Micromirror Device® as the switching element. Losses of 1.6 to 5.2 dB per bounce and crosstalk of -27 dB were also measured, both resulting primarily from diffraction from holes in each pixel and the inter-pixel gaps of the MEMS. © 2003 Optical Society of America

OCIS codes: 070.1170, 280.5110.

## 1. Introduction

There has been significant interest in using optics to generate true-time delay(s) (TTD)(s) for phased-array radars.<sup>1</sup> Many approaches have been proposed, including fiber delay lines,<sup>2-5</sup> wavelength division multiplexing,<sup>6-8</sup> Bragg gratings,<sup>9-12</sup> acousto optics,<sup>13</sup> waveguides,<sup>14-15</sup> optoelectronic integrated circuits,<sup>16</sup> and free-space approaches.<sup>17-21</sup>

Our work falls squarely in the free-space camp, with various optical TTD devices based on the White cell. The White cell is a system of three mirrors that constantly refocuses a bouncing beam to an array of spots. In our adaptation of the White cell, the spot array is produced on a spatial light modulator (SLM): one spot per pixel. The SLM is then used to choose between alternate paths for each beam, introducing time delays. One advantage to this scheme is that constant refocusing avoids the divergence problem, and thus avoids a large, cumbersome device. The key advantage, however, is that many beams can circulate in the device simultaneously, and each can be independently controlled. Thus the component

count is very low, requiring only one SLM, and a handful of mirrors and lenses.

We classify our devices as polynomial (meaning the number of delays available  $N$  is proportional to the number of bounces  $m$  a single beam makes on the SLM raised to some power) and exponential, meaning that  $N$  is proportional to some number raised to the power of  $m$ . Our scope here is polynomial cells. A demonstration of a linear cell was previously reported<sup>22</sup> in which the number of delays was proportional to  $m$ . This early design used a liquid-crystal SLM. Experimental results were presented previously for a quadratic cell ( $N \propto m^2$ ), also by using a liquid-crystal SLM.<sup>23</sup> A recent paper described designs for quadratic and higher-order polynomial cells based on microelectromechanical mirror technology.<sup>24</sup>

In this paper we report on an experimental demonstration of the simplest microelectromechanical systems- (MEMS)-based White cell TTD device, a linear cell. We used a commercially available MEMS device, the Texas Instruments Digital Micromirror Device (DMD®). We demonstrated proof-of-concept with six different switchable delays.

The organization of this paper is as follows: We start by reviewing the White cell operation on which our TTD cell is based. Then we show how to incorporate the MEMS mirror into the cell. We adapt the White cell to TTD by adding a second White cell and using the MEMS device to switch beams between them. Finally, we present our experimental data.

---

The authors are with the Department of Electrical Engineering, 205 Dreese Laboratory, The Ohio State University, 2015 Neil Avenue, Columbus, Ohio 43210.

Received 6 September 2002; revised manuscript received 1 November 2002.

0003-6935/03/081409-08\$15.00/0

© 2003 Optical Society of America

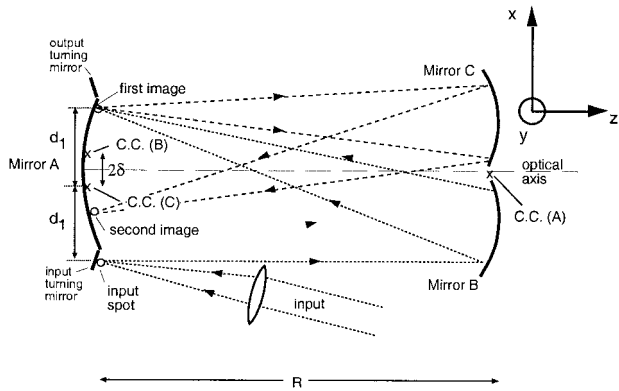


Fig. 1. Original White cell. The mirrors are separated by a distance equal to their radii of curvature  $R$ . The centers of curvature are shown. A spot on the input turning mirror is re-imaged by mirror B onto mirror A at the first image spot shown. From there the light goes to C, which creates a second image as indicated.

## 2. White Cell-Based True-Time Delay Device

The White cell, and its adaptation to optical TTD, has been explained in detail previously.<sup>22-24</sup> We will summarize it briefly here. A White cell<sup>25</sup> consists of three spherical concave mirrors of the same radius of curvature, as shown in Fig. 1. The mirrors are all separated by a distance equal to their common radius of curvature,  $R = 2f$ , where  $f$  is the focal length of the mirror. The center(s) of curvature (CC) of mirrors B and C are a distance  $\delta$  above and below the axis, respectively, and the CC of mirror A is halfway between mirrors B and C. With the spherical mirror design, a beam bounces between the mirrors multiple times to generate a long path while refocusing at each bounce. Because of the  $2f$  separation, a spot on mirror A will be imaged back onto mirror A by either mirrors B or C. In addition, mirror A images light from mirror B onto mirror C and vice versa.<sup>25</sup> Thus the beam is refocused without loss after each trip through the cell to a diffraction-limited spot, eliminating beam spreading.

A light beam circulating in the White cell produces a pattern of spots. The spot pattern is controlled entirely by the alignment of mirrors B and C. Each spot is re-imaged onto mirror A an equal and opposite distance about the center of curvature of the mirror to which it travels. Because these centers are separated by  $2\delta$ , each spot lands in a new location. The first two images are shown in Fig. 1. The input spot arrives a distance  $d_1$  below CC (B), and is re-imaged  $d_1$  above it. The second image is reflected about CC (C), appearing an equal distance from CC (C) on the other side of it. Many beams can circulate simultaneously, and each produces a unique set of spots. Figure 2 shows the spot patterns on mirror A for 36 input beams (two rows of 18 beams) each making nine bounces on mirror A. The bounce numbers are indicated. No spots from any input beam overlap with any other spots. The total number of bounces is fixed by the spacing between CC (B) and CC (C), and the size of mirror A.

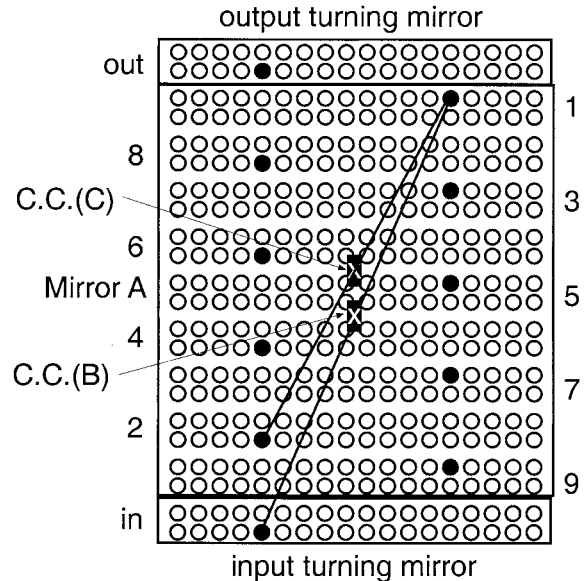


Fig. 2. Spot pattern for 36 spots, each making nine bounces on mirror A. A particular input spot is highlighted. Each spot appears an equal and opposite distance from the center of curvature of the spherical mirror from which the beam came last.

In a phased-array radar, there would be one light beam for each antenna element (or subarray). If each beam makes 20 bounces, then a single MEMS micromirror array having a  $400 \times 600$  pixel array can in principle control  $400 \times 600 / 20 = 12,000$  antennas. The ability to handle large numbers of light beams in a single device is a big advantage of the White cell approach, especially for controlling large antenna arrays.

To adapt the White cell to optical TTD, we replace mirror A with a SLM with a flat surface and a field lens in front of the SLM. The lens provides the imaging of the original mirror A (it images B onto C and C back onto B, avoiding diffraction loss), and the SLM is taken to be reflective. The field lens does not have to be adjacent to the SLM. We take the SLM in this case to be a MEMS two-state micromirror array, in which each micromirror can tip to one of two angles, here taken to be  $\pm 10^\circ$ . Figure 3 shows the MEMS at the left-hand side, with every micromirror tipped to  $-10^\circ$ , and two spherical mirrors at the right-hand side. There is a separate field lens for each mirror, the reason for which will become evident shortly. We place mirror C on an axis normal to the MEMS mirror plane, and mirror B along an axis at  $-20^\circ$ . Thus light coming from C, and striking a pixel tipped to  $-10^\circ$ , is reflected to B, and vice versa. That is, mirrors B, C, and the MEMS/lenses combination form a White cell. Beams circulating in this White cell trace out the spot patterns as dictated by the alignment of B and C. The spots are aligned to land on individual pixels. Thus on each bounce, a beam strikes a new micromirror.

We can choose to allow a given beam to continue bouncing in the B-C White cell by leaving all micromirrors in the  $-10^\circ$  position, or we can switch it

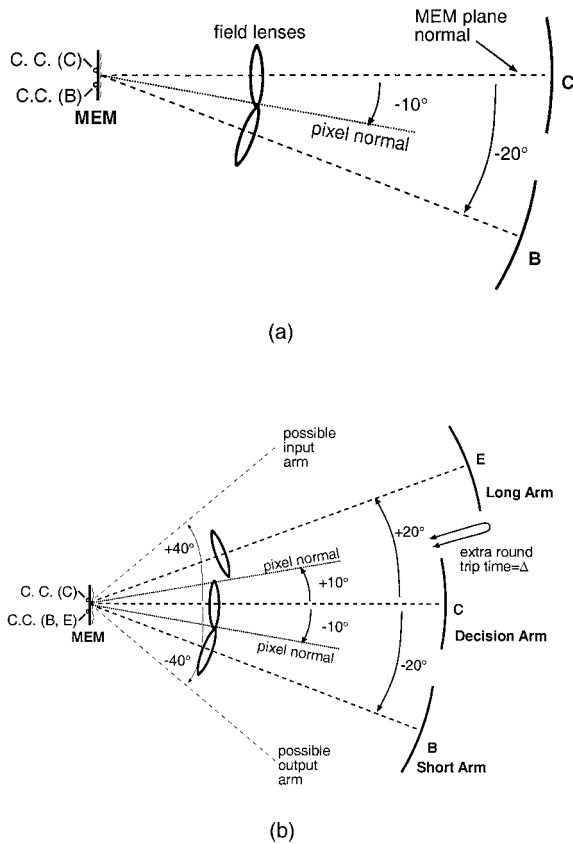


Fig. 3. (a) White cell is formed by the flat MEMS micromirror array, two field lenses, and two spherical mirrors. In this picture, if every pixel is tipped to  $-10^\circ$ , the beams circulate in this White cell, striking a new pixel on every bounce. (b) Linear cell optical TTD cell using a 2-state MEMS tip/tilt micromirror array. Mirrors B and C form one White cell with the MEMS device, and mirrors C and E form another. The CC of mirrors B and E are co-aligned, so the spot pattern is the same regardless of which White cell is visited on any particular bounce.

out by tilting one micromirror to the other position at  $+10^\circ$ .

Now, we add another arm to the cell, also shown in Fig. 3, along an axis at  $+20^\circ$  to the MEMS mirror normal. This arm, containing mirror E, is longer than the arms containing mirrors B and C. If light is coming from C, and the appropriate micromirror is tipped to  $+10^\circ$ , the light beam is sent to mirror E, and when the light returns to the MEMS mirror, that next micromirror is also tipped to  $+10^\circ$ . Two bounces are required for each visit to mirror E. Mirrors C and E make up a second, longer White cell. Note that the two White cells share the arm containing mirror C.

Mirror E's CC is co-aligned with that of mirror B, so that regardless of which of the two White cells the light is sent to, the spot pattern is identical.

We call the arm containing mirror B the short arm, and the arm containing mirror E the long arm. The arm that is shared by both White cells, the one containing mirror C, is called the decision arm. This is because, at this point, the decision is made on each

pass whether to create one unit of delay by passing to the long arm or to create no delay by passing to the short arm.

Note that to meet the imaging requirements, the long arm requires a lens with a different focal length than the other two arms. For this reason, we use a separate lens for each arm of the cell. The appropriate imaging conditions are maintained when the distance from the field lens to the mirror is equal to the focal length of the field lens.<sup>23</sup>

Now, every beam makes a fixed number of bounces  $m$  through the device, and after  $m$  bounces every beam will exit the device. Changing the number of times a given beam passes to the long arm as compared with the number of visits to the short arm varies the time of flight of each individual light beam. The shortest time delay possible is obtained when a given beam circulates between B and C for all  $m$  bounces. This delay is common to all beams, and is thus in effect subtracted out. The path-length difference between the long and short arms determines the delay increment  $\Delta$ . Because the beam always travels to the decision arm as part of a transit path, this length represents a constant contribution to the transit time. Therefore, the total net time delay is given by

$$T_{\text{delay}} = n(T_{\text{long}} - T_{\text{short}}) = n\Delta, \quad (1)$$

where  $n$  is the number of bounces off of mirror E,  $T_{[\text{long}(\text{short})]}$  is the round-trip transit time through the corresponding arm, and  $\Delta$  is the time-delay increment.

A beam sent to the long arm one time will have a delay of one increment, a beam sent to the long arm twice will have a delay of two increments, and so forth. Note that the beam may only be sent to mirror E on every other bounce (it cannot go there from B, only from C). The maximum number of delays  $N$  that can be obtained is

$$N = \frac{m}{2}. \quad (2)$$

Thus this is a linear cell, meaning the number of delays is proportional to the number of bounces. Of course, the number of delays obtainable with a realistic number of bounces in a linear cell is far too small to be useful for a real radar. Optical true-time delay devices based on the White cell with far higher capability, up to 6,550 delays in 18 bounces, have been proposed elsewhere.<sup>24</sup> Those designs assume a three-state micromirror array. The linear cell is useful, however, as a proof-of-concept demonstration.

#### A. Input and Output

Although the conventional way for light to enter and exit a White cell is by way of input and output turning mirrors, it is possible to use the MEMS pixels themselves for this purpose. We can create additional arms along angles of  $\pm 40^\circ$  with respect to the MEMS device normal, also shown in Fig. 3. A beam enters

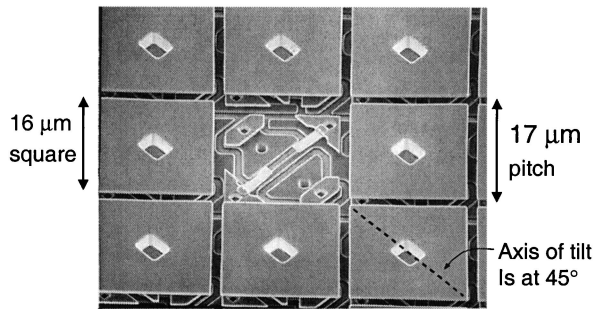


Fig. 4. Photomicrograph of a section of the MEM (Texas Instruments DMD®) micromirror array. The entire chip has  $400 \times 600$  pixels.<sup>26</sup>

via the  $+40^\circ$  arm, and is configured to produce a spot on a particular pixel. The micromirror at that pixel is rotated to  $+10^\circ$ , sending the beam next to mirror B. The next pixel micromirror is set to  $-10^\circ$ , and the beam goes to the decision arm. The beam is now said to be in the cell, and the input sequence required two additional bounces on the MEMS mirror array. Similarly, a beam can be made to exit by tilting a pixel after the decision arm to  $+10^\circ$ , sending the beam to mirror E, and thence to a pixel tilted to  $-10^\circ$ , which sends the light out of the output arm. Thus if the input and output turning mirrors are replaced by the MEMS pixels, an extra four bounces are required. Because all beams will follow the same input and output path (albeit via different pixels), the extra delay incurred is common to all light beams and will not affect the antenna-array steering.

### 3. Apparatus

#### A. Apparatus Design

We have built and demonstrated the design presented above. In our apparatus, we used a MEMS device developed by Texas Instruments (TI) for use in portable computer projector systems. Although much development work in micromirror array is going on, at the time of this writing, TI still, after many years, has the only truly large array of tipping micromirrors that is commercially available. The device, called a Digital Micromirror Device (DMD®) consists of an array of  $600 \times 800$  tiny micromirrors that can be tilted to  $\pm 10^\circ$  by an applied voltage. The pixels are  $16 \mu\text{m}$  square and are arrayed on  $17 \mu\text{m}$  centers. They rotate around their diagonals on a hollow support post, which appears as a  $3.2 \mu\text{m}$  hole in the center of each pixel. Figure 4 shows nine of the pixels.<sup>26</sup> One mirror has been removed to show the mechanism underneath. The DMD® is micro-machined on top of a silicon memory circuit and operates with standard complementary metal-oxide semiconductor (CMOS) voltage levels.<sup>27</sup> Because of the tip angle of the pixels, the arms in the White cells are separated by an angle of  $\pm 20^\circ$ .

Because one cannot buy a DMD® chip outright, we bought a computer projector (CTX Model EzPro 700), and used the projector electronics to control the

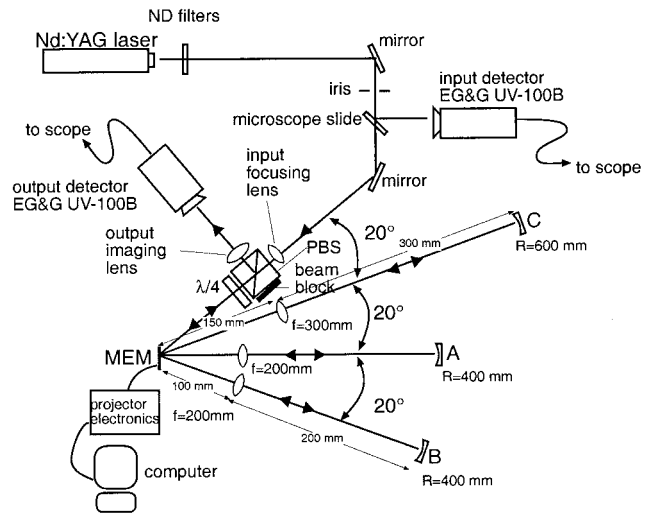


Fig. 5. The apparatus.

DMD®. In Subsection 3.B we will discuss the projector in more detail. For now we observe that because it is intended to display computer screens, to address a particular pixel one needs only to select that pixel on a computer screen, and ask for it to be projected. Thus pixels to be turned to  $+10^\circ$  were all drawn on the computer screen as white, and the pixels to be turned to the other angle,  $-10^\circ$ , were set to black.

The rest of the apparatus is shown in Fig. 5. The source was a pulsed Nd:YAG, whose  $1.06 \mu\text{m}$  output was frequency-doubled to a green line at  $532 \text{ nm}$ . The pulses had a 5-ns rise time and were externally triggered, as we will discuss later. Neutral density (ND) filters were used to attenuate the beam to a safe level. We used an iris to shape the input beam and a lens to focus the beam onto the MEMS micromirror array. A microscope slide was used as a beamsplitter to pick off some of the input power to obtain an input reference pulse.

Our original intention was to bring the input beams in along the  $+40^\circ$  arm, and have them exit the cell along a  $-40^\circ$  arm. We found, however, that the Fresnel reflection of the input beam from the uncoated cover glass of the MEMS device, the reflection also going into the  $-40^\circ$  arm, obscured our readings. Thus we re-used the input arm for output. A polarizing beam splitter (PBS) was used in combination with a quarter-wave ( $\lambda/4$ ) plate to separate the input and output beams. This polarization dependence is undesirable but can be avoided with a better choice of input and output directions. Another lens focuses the output beam onto the output detector.

For the TDD itself, there are several imaging conditions that must be maintained.<sup>23</sup> The MEMS mirror array must image onto itself via any of the paths through each of the mirrors B, C, and E. Also, C must image onto both B and E. We arbitrarily chose the short and decision arms to be the same length for ease of design. These arms have spherical mirrors of  $R = 400 \text{ mm}$ , and field lenses of  $f = 200 \text{ mm}$ . The distances are shown.

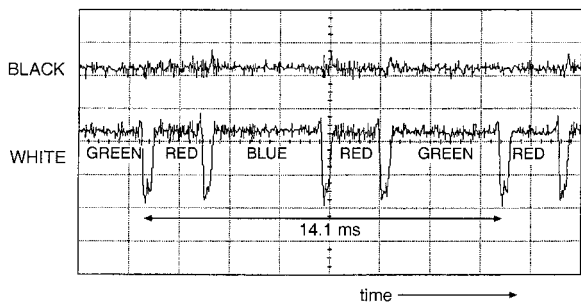


Fig. 6. Timing of the pixels in the computer projector.

Our delay increment was chosen to be 1 ns, so the long arm was 150 mm longer than the short arm. Thus mirror E had a radius of curvature  $R = 600$  mm, and the corresponding field lens had a focal length of 300 mm.

The pixel size on the TI DMD® is only  $16 \mu\text{m}$ ; it is difficult to focus and align a spot small enough to fit on a single pixel (and the hole then would create large losses). We mitigated this problem by using macropixels, regions on the micromirror array of  $50 \times 50$  pixels. All the micromirrors in any one macropixel are set to the same state; thus we can use a considerably larger spot size. The downside is diffraction and fill-factor losses from the holes in the mirrors and the spaces between them.

In our demonstration, we used 16 bounces. Because four of those are used for input and output, from Eq. (2), with 12 remaining bounces there were six possible incremental delays.

#### B. Synchronizing the MEMS Micromirrors

As mentioned earlier, we used a computer projector to drive the MEMS mirror array. In the projectors, however, the pixels are not driven to a particular position and left there until there is a change in the display. To avoid stiction, the pixels are flipped pe-

riodically. Further, in this projector a single MEMS chip is used to project color images by synchronizing red, green, and blue information with a spinning color wheel. Finally, gray scale is obtained by varying the duty cycle. We characterized the pixel motion by reflecting a laser beam from it and imaging a single pixel onto a detector. Figure 6 shows the timing of the color signals and the release flipping. The upper trace shows the reflected light when black is selected. The lower trace shows that the pixels are flipped periodically. We then used a signal tapped off the color wheel signal in the projector to trigger our laser pulses, introducing the appropriate delay to time the pulses correctly.

## 4. Data

### A. Delay Measurements

We measured delays from zero to 5 nanoseconds in 1-nanosecond increments. We show the first 4 nanosecond increments in Fig. 7. A reference detector measures the input beam before it enters the cell (labeled input detector in Fig. 5). The output detector measures the output pulse after propagating in the cell. The output traces have been superimposed to view the delays more easily. Their timings are referenced to the input pulse (not shown). There are five traces, corresponding to five different pixel settings.

The solid vertical line shows the timing of the output pulse if no delay is selected. This is the delay to which all other delays are referenced. The dashed lines indicate the peaks for the delayed traces. The vertical scale is 10 mV/div and the time axis is set at 2 ns/div.

The signal with no delay has a peak magnitude of approximately 60 mV, whereas the signal with 4 nanoseconds of delay has a peak magnitude of approximately 35 mV. The number of bounces in the

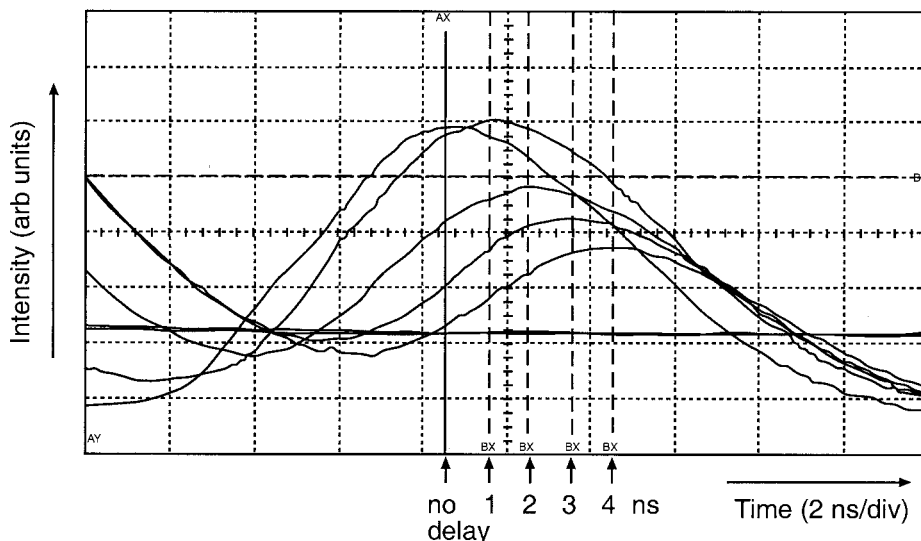


Fig. 7. Time delay measurements, showing delays of zero through 4 ns. Delay of 5 ns not shown.

cell is the same for all traces, and therefore all the output pulses should experience the same loss and have the same amplitude. What is in fact happening is that the beam expands on its way to the spherical mirrors (see Fig. 1). Spherical mirror E is the same diameter as B and C, and thus generates slightly higher diffraction losses. Normally, diffraction losses will be negligible, because the spherical mirrors image onto each other. As we discuss below, there is a great deal of diffraction from features on the MEMS mirror array itself in this particular case.

### B. Crosstalk

There are two types of crosstalk that would be of interest in a device like this. One is the inter-element crosstalk, the amount of light belonging to one antenna element that leaks into a path leading to another antenna element. For example, if a spot on a given micromirror overlapped onto another pixel belonging to a different light beam, this type of crosstalk would result. Because we had only one input beam available, we did not measure inter-element crosstalk.

The second type of crosstalk is within a single light beam—the amount of light leaking into the wrong arm on a given pass. This intra-element crosstalk causes some energy to appear at the wrong time even though it is delivered to the correct antenna element. This type of crosstalk would result, for example, if the divergence angles of the beams leaving mirror A were greater than the angles between the different arms. The angle between arms is constrained to twice the micromirror tilt angle, in this case to  $20^\circ$ .

Ideally, the diffraction is limited to beam spreading from a Gaussian beam and is controlled by the spot size. With this particular apparatus, however, the spots cover a large number of micromirrors, so we have additional diffraction from both the spaces between the micromirrors and the holes in the mirrors themselves.

The amount of intra-element crosstalk by use of this particular MEMS mirror array is thus based on the diffraction angle of a beam reflecting off of an array of  $16\text{-}\mu\text{m}$  square pixels with a  $3.2\text{-}\mu\text{m}$  square hole and  $1\text{-}\mu\text{m}$  gaps. We calculated this diffraction pattern, and found that the half angle within which 95% of the energy is kept was approximately  $17^\circ$  full angle. The arms of the cell are separated by  $20^\circ$ , so the crosstalk should be small. The edge of the decision lens, however, is only  $12^\circ$  from the center of the short-arm lens, meaning it can capture some of the remaining 5% of the light and send it to the wrong arm.

We measured the intra-element crosstalk for one bounce as follows: A detector was placed first in the decision arm, with a lens to focus all the light entering this arm onto the detector. The beam was then sent to a different arm (the short arm). The leakage into the decision arm was approximately  $-27$  dB.

### C. Loss

There are two major sources of optical loss in the experimental apparatus: the reflection losses from each bounce on the micromirror array, and diffraction losses caused by the field lenses truncating the diffraction pattern from the micromirrors. Fresnel losses from the anti-reflection coatings from the lenses ( $T = 0.95$ ) and loss from the mirrors ( $R = 0.995$ ) are negligible by comparison.

The micromirror array reflection losses have three major components: reflectivity loss,  $R$ , due to the aluminum used in the micromirrors ( $R = 0.9$  at our wavelength), fill-factor loss caused by the holes and the gaps between the pixels (fill factor = 89%),<sup>27</sup> and truncation losses if the beam spots are larger than the macropixels. In our case the beams were, in fact, larger than the  $50 \times 50$  macropixels, and we measured the truncation loss to be 0.3 dB. This was done by placing a lens and a detector to capture the light reflected from the micromirror array. We then switched the macropixel to white against a field of black and compared the power to the case where the entire micromirror array area was set to white. The total reflection losses from these three effects predict 1.26 dB per bounce to the total loss.

The diffraction from the inter-element spaces and holes in the mirrors, discussed earlier, also causes loss. We measured these by placing a lens and a detector in each arm one after the other. This test lens was larger in diameter than the White cell optics, and so would capture all light that makes it into a given arm. Going from the input beam to the short arm, we found a total loss of 1.6 dB; going from the short arm to the decision arm gave a loss of 5.2 dB, and 4.0 dB going from the decision arm to the long arm. These include the reflection losses discussed above. Also, we measured a cumulative total loss of over 12 dB with just one pass to each of the three arms in the cell. That includes three bounces off the MEMS device, and the remaining 8.4 dB is then caused by diffraction losses.

Some comments on the loss measurements are in order. The primary source of loss in the White cell TTD device was from the micromirror array, which is to be expected because we are using it in a manner and for an application for which it is not intended. A MEMS mirror designed for optical TTD would ideally have gold mirrors to improve reflectivity at the infrared wavelengths at which TTDs are expected to operate, have pixels larger than the spot size to avoid truncation loss, and would not have holes in the mirrors, and thus would avoid diffraction losses. Holes may be unavoidable, however, because in the manufacture of MEMS devices some kind of holes or spaces are required to allow the release layer to be dissolved and removed, particularly if the pixels are large. MEMS device manufacturers today predict reflection losses as low as 0.1 dB. With a good design of an optical TTD based on MEMS tip/tilt micromirror arrays one should be able to hold insertion loss to just

a few dB, even with a large number of bounces. In other work,<sup>23</sup> we found losses apart from the SLM to be negligible, confirming our claim that diffraction losses can be made small.

## 5. Summary and Discussion

We have experimentally demonstrated that optical true-timed delay devices based on the White cell can be built using microelectromechanical mirror arrays. In our proof-of-concept demonstration, we have demonstrated six differential delays in nanosecond increments.

Both crosstalk and loss were measured, and although both are higher than they should be, both can be corrected with proper design. The crosstalk in our apparatus was approximately  $-27$  dB between adjacent arms, due to field lenses extending into the beams of other arms. The loss was approximately 1.2 dB for each bounce off the MEMS mirror, which is attributed to fill factor, metal-reflectivity loss, and diffraction from the holes in the micromirrors and the gaps between them. Other losses were primarily due to the diffraction losses caused by a wide-angle diffraction pattern and the resulting truncation of the beams by the lenses and mirrors. These can be reduced to some extent by use of optical components with larger diameters. Both the loss and the crosstalk could be improved if digital tip/tilt MEMS devices with larger pixels and no holes could be obtained.

In this simple linear cell, the number of delays is very small. Optical TTD devices based on the White cell producing up to 6,550 delays in 18 bounces have been proposed elsewhere.<sup>24</sup> Those designs assume a three-state tipping micromirror array, a device that is under development<sup>28</sup> but not currently available. The goal of the present work was to establish proof-of-concept.

The White cell approach offers the possibility of producing a very large range of delays (thousands of delays) for a very large number (thousands) of antenna elements, with a single MEMS device and a few lenses and mirrors. Once appropriate MEMS micromirror arrays become commercially available, these devices are attractive in general because of their compact size, low cost, polarization independence, and most importantly, robustness in nonlaboratory environments.

The authors gratefully acknowledge the participation and assistance provided by Stuart A. Collins, Jr., of The Ohio State University. This work is based on ideas developed by him.

## References

1. H. Zmuda and E. N. Toughlian, "Photonic aspects of modern radar," in *The Artech House Optoelectronics Library*, B. Culshaw, A. Rogers, and H. Taylor, eds., (Artech House, Norwood, Mass., 1994) pp. 550.
2. W. Ng and A. A. Watson, "The first demonstration of an optically steered microwave phased array antenna using true-time-delay," *J. Lightwave Technol.* **8**, 1124–1131 (1991).
3. A. P. Goutzoulis and D. K. Davies, "Hardware-compressive 2-D fiber optic delay line architecture for time steering of phased-array antennas," *Appl. Opt.* **29**, 5353–5359 (1990).
4. P. J. Matthews, M. Y. Frankel, and R. D. Esman, "A wide-band fiber-optic true time-steered array receiver capable of multiple independent simultaneous beams," *IEEE Photon. Technol. Lett.* **10**, 722–724 (1998).
5. H. Zmuda, E. N. Toughlian, P. Payson, and H. W. Klumpke III, "A photonic implementation of a wide-band nulling system for phased arrays," *IEEE Photon. Technol. Lett.* **10**, 725–727 (1998).
6. A. P. Goutzoulis, D. K. Davies, and J. M. Zomp, "Hybrid electronic fiber optic wavelength-multiplexed system for true time-delay steering of phased array antennas," *Opt. Eng.* **31**, 2312–2322 (1992).
7. A. P. Goutzoulis and J. M. Zomp, "Development and field demonstration of an eight-element receive wavelength-multiplexed true-time-delay steering system," *Appl. Opt.* **36**, 7315–7326 (1997).
8. R. Taylor and S. Forrest, "Steering of an optically-driven true-time delay phased-array antenna based on a broad-band coherent WDM architecture," *IEEE Photon. Technol. Lett.* **10**, 144–146 (1998).
9. G. A. Ball, W. H. Glenn, and W. W. Morey, "Programmable fiber optic delay line," *IEEE Photon. Technol. Lett.* **6**, 741–743 (1994).
10. D. A. Cohen, Y. Chang, A. G. J. Levi, H. R. Fetterman, and I. L. Newberg, "Optically controlled serially fed phased array sensor," *IEEE Photon. Technol. Lett.* **8**, 1683–1685 (1996).
11. B. Tsap, Y. Chang, H. R. Fetterman, A. F. J. Levi, D. A. Cohen, and I. Newberg, "Phased-array optically controlled receiver using a serial feed," *IEEE Photon. Technol. Lett.* **10**, 267–269 (1998).
12. J. L. Cruz, L. Dong, S. Barcelso, and L. Reekie, "Fiber Bragg gratings with various chirp profiles made in etched tapers," *Appl. Opt.* **35**, 6781–6787 (1996).
13. M. Tamburrini, M. Parent, L. Goldberg, and D. Stillwell, "Optical feed for a phased array microwave antenna," *Electron. Lett.* **23**, 680–681 (1987).
14. Z. Fu, C. Zhou, and R. T. Chen, "Waveguide-hologram-based wavelength-division multiplexed pseudoanalog true-time-delay module for wide-band phased array antennas," *Appl. Opt.* **38**, 3053–3059 (1999).
15. R. L. Q. Li, X. Fu, and R. Chen, "High packing density 2.5 THz true-time delay lines using spatially multiplexed substrate guided waves in conjunction with volume holograms on a single substrate," *J. Lightwave Technol.* **15**, 2253–2258 (1997).
16. L. Eldada, "Laser-fabricated delay lines in GaAs for optically steered phased-array radar," *J. Lightwave Technol.* **13**, 2034–2039 (1995).
17. X. S. Yao and L. Maleki, "A novel 2-D programmable photonic time-delay device for millimeter-wave signal processing applications," *IEEE Photon. Technol. Lett.* **6**, 1463–1465 (1994).
18. N. Madamopoulos and N. Riza, "Directly modulated semiconductor-laser-fed photonic delay line with ferroelectric liquid crystals," *Appl. Opt.* **37**, 1407–1416 (1998).
19. N. A. Riza, "25-Channel nematic liquid-crystal optical time-delay unit characterization," *IEEE Photon. Technol. Lett.* **7**, 1285–1287 (1995).
20. D. Dolfi and P. Joffre, "Experimental demonstration of a phased-array antenna optically controlled with phase and time delays," *Appl. Opt.* **8**, 1824–1828 (1996).
21. E. N. Toughlian and H. Zmuda, "A photonic variable RF delay line for phased array antennas," *J. Lightwave Technol.* **8**, 1824–1828 (1990).
22. B. L. Anderson, S. A. Collins, Jr., C. A. Klein, E. A. Beecher,

- and S. B. Brown, "Optically produced true-time delays for phased antenna arrays," *Appl. Opt.* **36**, 8493–8503 (1997).
23. B. L. Anderson and C. D. Liddle, "Optical true-time delay for phased array antennas: demonstration of a quadratic White cell," *Appl. Opt.* **41**, 4912–4921 (2002).
  24. B. L. Anderson and R. Mital, "Polynomial-based optical true-time delay devices with microelectromechanical mirror arrays," *Appl. Opt.* **41**, 5449–5461 (2002).
  25. J. White, "Long optical paths of large aperture," *J. Opt. Soc. Am.* **32**, 285–288 (1942).
  26. Texas Instruments, DLP<sup>™</sup> newsletters. [http://www.dlp.com/about\\_dlp/about\\_dlp\\_images\\_pixels\\_micro.asp](http://www.dlp.com/about_dlp/about_dlp_images_pixels_micro.asp).
  27. L. J. Hornbeck, "Digital Light Processing<sup>™</sup> for high-brightness, high-resolution applications," presented at Electronic Imaging '97, San Jose, California, 1997.
  28. O. Blum Spahn, E. J. Garcia, V. Easch, G. Grossetete, F. Bitsie, S. Mani, J. Jakubaszak, "Optical performance of pivoting micromirrors," in *Proc. SPIE Micromachining and Microfabrication Process Technology VII*, **4561**, Jean Michel Karam, John Yasaitis, eds., 283–292 (2001).